

UNSUPERVISED DATA-DRIVEN NUCLEI SEGMENTATION FOR HISTOLOGY IMAGES

Vasileios Magoulanis, Peida Han, Yijing Yang, C.-C. Jay Kuo

University of Southern California, Los Angeles, California, USA

ABSTRACT

An unsupervised data-driven nuclei segmentation method for histology images, called CBM, is proposed in this work. CBM consists of three modules applied in a block-wise manner: 1) data-driven color transform for energy compaction and dimension reduction, 2) data-driven binarization, and 3) incorporation of geometric priors with morphological processing. CBM comes from the first letter of the three modules – “Color transform”, “Binarization” and “Morphological processing”. Experiments on the MoNuSeg dataset validate the effectiveness of the proposed CBM method. CBM outperforms all other unsupervised methods and offers a competitive standing among supervised models based on the Aggregated Jaccard Index (AJI) metric.

Index Terms— Histology images, Nuclear segmentation, Color Transform, Unsupervised, Morphological Processing

1. INTRODUCTION

Histology images provide strong cues to pathologists in cancer diagnosis and treatment. Automated nuclei instance-level segmentation for histology images provides not only the number, density and sizes of nuclei but also morphological features, such as the magnitude and the cytoplasmic ratio. This information facilitates cancer diagnosis and assessment of the tumor aggressiveness rate. Nuclei segmentation tasks can be conducted in a supervised or an unsupervised manner. For supervised methods, the annotation of high resolution histology images in pixel-level accuracy is a time-consuming job, being carried out by expertized physicians. Other identified challenges include the variability of cell appearance from different organs, unclear boundaries, as well as color and intensity variations in stained images from different laboratories. Furthermore, it is a subjective task and annotated labels tend to vary from one person to the other. All the above factors challenge the practical generalizability of supervised segmentation methods, as histology images become larger in their number and more diversified in content.

Earlier methods on nuclei segmentation were mainly unsupervised. They were based on thresholding [1, 2], mathematical morphology for robust feature extraction [3], or statistical modeling for segmentation and likelihood maximization for boundary refinement [4]. Another popular tool was

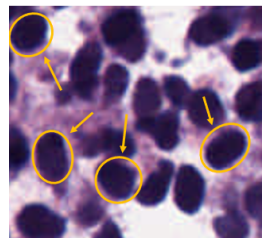


Fig. 1. Illustration of nuclei cell appearance in histology images.

the watershed algorithm, which was combined with various ways for extracting potential nuclei locations [5, 6]. Moreover, a work by Ali *et al.* [7] proposed an adaptive active contour mechanism that takes boundary- and region-based energy terms of the cell into account.

Recently, deep-learning-based (DL) methods [8, 9, 10, 11] have been applied to this problem. A wide variety of DL models are trained by human labeled data. In general, supervised methods provide significantly better performance than the unsupervised ones. The motivation of our research stems from the fact that nuclei instance labeling is a fairly laborious task, with reportedly highly subjective annotations and miss-labeling rate [12] that challenges the supervised solutions. Several studies have been made to mitigate the labeling cost. For example, Qu *et al.* [13] proposed a two-stage learning framework using coarse labels. Other researchers [14, 15] investigated the self-supervised DL method to reduce the number of required labeled data by exploiting the observation that nuclei size and texture can determine the magnification scale. Besides, there is a domain shift problem [16] arising from stain and nuclei variations in histology images of different organs, patients and acquisition protocols.

In spite of the high performance, DL-based solutions have their own shortcomings on top of the high labeling cost. First, they are perceived as a “black-box” approach. Interpretable solutions are highly desired in medical applications as they enable explainable decisions and the tools are more trustworthy in clinical use. Second, they bear a high computational cost in training and testing [17] because of a large number of parameters in order to achieve a certain performance.

In this work, we propose an unsupervised data-driven

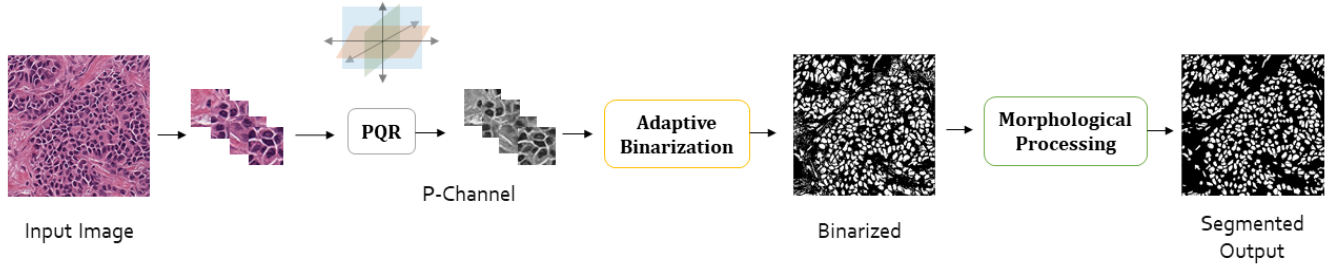


Fig. 2. An overview of the proposed CBM method.

method to solve the nuclei segmentation problem. The solution consists of three modules applied to each image block of size 50×50 : 1) data-driven color transform for energy compaction and dimension reduction, 2) data-driven binarization, and 3) incorporation of geometric priors with morphological image processing. It is named “CBM” because of the first letter of the three modules – “Color transform”, “Binarization” and “Morphological processing”.

We conduct experiments on the MoNuSeg dataset to demonstrate the effectiveness of the proposed CBM method. It outperforms all other unsupervised approaches and stands in a competitive position with supervised ones based on the Aggregated Jaccard Index (AJI) performance metric. Thus, the proposed CBM method is an attractive solution in practice nuclei segmentation, since it yields comparable performance with state-of-the-art supervised methods while requiring no training labels.

2. PROPOSED CBM METHOD

Each histology test image of the experimenting dataset has a spatial resolution of 1000×1000 pixels and each pixel has R, G and B three color channels. We partition each image into nonoverlapping blocks of size 50×50 pixels and apply contrast enhancement to accentuate the boundaries around nuclei as a pre-processing step. Then, CBM processes each block independently with three modules as elaborated below.

2.1. Data-Driven Color Transform

Nuclei segmentation is a binary decision problem for each pixel; namely, it belongs to either the nucleus or the background region. We need pixel attributes to make decision. A pixel has R/G/B color values in raw histology images. There exist strong correlations between RGB channels in histology images as shown in Fig. 3(a). We can exploit this property for energy compaction.

There are many well-known color spaces such as YUV, LAB, HVS, etc. However, they are not data-dependent color transforms. To achieve optimal energy compaction, we apply the principal component analysis (PCA) to the RGB 3D color vector of pixels inside one block. That is, we can determine the covariance matrix between the R/G/B color components

based on pixels in the region. Then, the three eigenvectors define the optimal transform and their associated eigenvalues indicate the energy distributions among the three channels. The transform output channels are named P , Q and R channels. They are channels of the first, the second and the last components, respectively.

The energy distributions of three color components of the RGB, LAB and PQR color spaces for a representative histology image is shown in Table 1, where the P/Q/R channel energy distribution is averaged over all blocks in one image. As shown in the table, the first principal component, P , has an extremely high energy percentage while the rest two components have very limited energy. As a result, we can treat the latter two as background noise and discard them. Instead of considering segmentation using three attributes, we simplify it greatly using a single attribute. As the first principal subspace, P points at the direction where the variance is maximized. It better captures the transition from background to nuclei cell areas, thus leading to a more distinct local histogram.

We normalize raw P -channel values to the range of $[0, 1]$ with linear scaling. Note that, if \mathbf{x} is an eigenvector of the covariance matrix of RGB color channels, $-\mathbf{x}$ is also an eigenvector. We choose the one that maps a higher P value to background (i.e., brighter) and a lower P value to nuclei (i.e., darker). This can be easily achieved by imposing the P value to be consistent with the luminance value in the LAB color space, since the background luminance is higher than those of nuclei. The original color and the normalized P -channel representations for a block are compared in Fig. 3. Performance using the P channel against the L channel (in the LAB color space) will be compared in Sec. 3.

Table 1. Energy distribution of three channels of three color spaces in a representative histology image.

RGB	LAB	PQR
38.1% (R)	29.3% (L)	97.7% (P)
27.2% (G)	40.1% (A)	1.9% (Q)
34.7% (B)	30.6% (B)	0.4% (R)

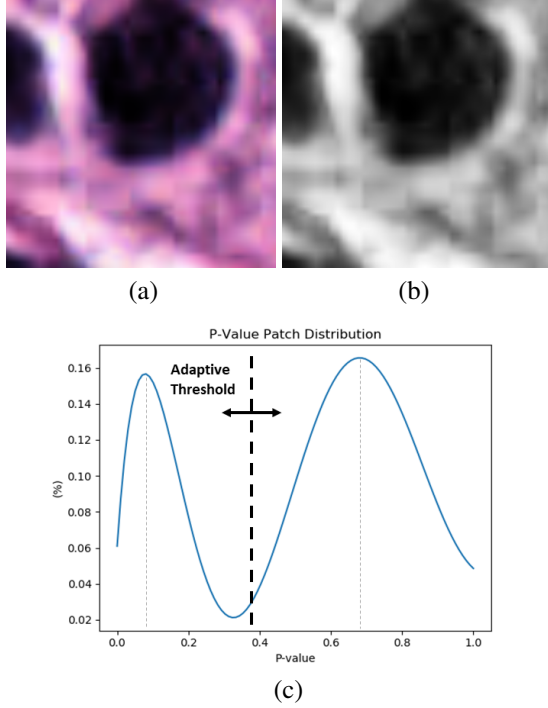


Fig. 3. Comparison of two representations in a block image: (a) R/G/B color and (b) P value in gray and (c) its corresponding bi-modal histogram.

One can see that the energy compaction capability of $P/Q/R$ depends on color homogeneity in a region. In most images, as the block size grows larger, the P -channel energy compaction property becomes lower. This is attributed to the fact that the color distribution of a larger block is less homogeneous and the correlation structure is more complicated.

2.2. Data-Driven Binarization

To conduct the binary classification of pixels, we study the histogram of the P value of each pixel in a block. A representative histogram is shown in Fig. 3(c), which has a bi-modal distribution. The modality in the left is contributed by the P values of pixels in the nuclei region while that in the right comes from the P values of pixels in the background region. There exists a valley between the two peaks, which are from pixels lying on transitional boundaries between nuclei and background. Thus, binarization can be achieved by identifying the intermediate point in between the two modalities and use the associated P value as the adaptive threshold, which is denoted by T . A pixel of P value is classified to the background region if $P > T$ and the nuclei region if $P \leq T$. Since threshold T is determined by the histogram of the P value of pixels in a block, the binarization process is fundamentally an adaptive thresholding method. Whether it will yield a successful outcome depends on the bi-modal histogram assumption.

The bi-modal histogram assumption holds under the fol-

lowing two conditions:

1. if the block size is not too large,
2. if the ratio of the nuclei pixel number and the background pixel number does not deviate much from unity.

In case the first condition is not met, we may see K -modalities with $K > 2$. Then, there are multiple valley points, which makes the threshold selection challenging. If the second condition is not met, it means that the majority of pixels belong to one of two classes and we may see one dominant modality while the second modality is weak. Because it is difficult to choose a robust threshold under the first condition, we partition one block of size 50×50 into four sub-blocks of size 25×25 and conduct the data-driven color transform and binarization in each of the four sub-blocks. On the other hand, if the second condition happens, we merge 4 blocks into a super-block of size 100×100 and conduct the same processing in the super-block.

2.3. Morphological Processing

We have so far concentrated on pixel classification based on its color attributes in the first two modules of the CBM method. Now, we would like to take the neighborhood of a pixel into account. Typically, nuclei appear in form of rounded blobs (i.e., convex objects). Yet, we observe the following three common errors after the second module:

- (a) nuclei instances may be falsely connected,
- (b) false positives may appear because of the staining process,
- (c) holes exist inside the nuclei cell because of the inner intensity variations.

For (a), we can split the larger ones using the convex hull algorithm to find high convexity areas that imply an underlying connectivity between two cells. For (b), we can filter out abnormally small nuclei in the first place based on the prior knowledge on the average area of a nucleus. For (c), the hole filling filter is used to correct the false negatives inside the nuclei cell. For some images with dense cell areas and blurred boundaries, the connectivity may be more severe, having bundled together more than two cells. We found that, after applying the previous procedure in an iterative manner, the performance further increases. Thus, we repeatedly remove small cells and split larger pieces—with relatively high convexity areas—, until no further changes in the full image. The effect of this processing is illustrated in an example as shown in Fig. 4.

3. EXPERIMENTAL RESULTS

The data from the 2018 MICCAI MoNuSeg Challenge [9] are used to evaluate the performance of our proposed CBM

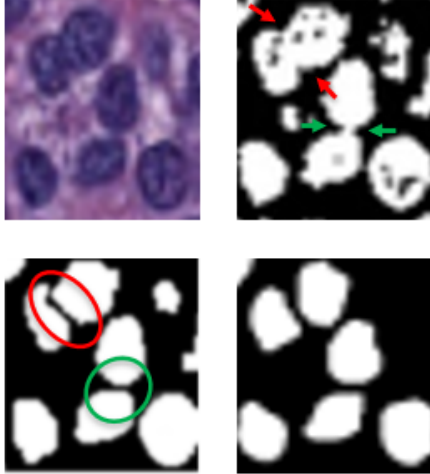


Fig. 4. Visualization of the morphological processing effect: input block (upper left), noisy binarized output (upper right), an improved result by splitting two distinct nuclei (bottom left), and segmentation ground-truth (bottom right).

method. This is a popular dataset for existing work, providing also different testing configurations. For the validation purpose, we follow the data splitting as suggested in [9].

For performance benchmarking with other existing works, we report the results on the 6 histology images set from bladder, colon, stomach, referred as Test-2, as well as the test data from the challenge set (14 images from various organs) in Table 2, where the commonly used AJI metric [9] is adopted. The AJI metric is more accurate for instance-level segmentation tasks by taking both the nuclei level detection and pixel-level error performance into account.

As shown in the table, our method outperforms all other unsupervised ones by a large margin in either testing scenarios. Notably, the gap is large even for the DL-based unsupervised approach denoted by “self-supervised” [14] in the table. As compared with supervised methods, CBM stands at a competitive position. It achieves similar performance with sophisticated models such as BES-Net [20]. It is also worthwhile to emphasize that most of the supervised methods use expensive models as a backbone architecture (in terms of the number of its parameters) such as Res-Net or Dense-Net. Instead, CBM is a parameter-free method with simple components. Its computational complexity is significantly lower.

It is also evident from Table 2 that supervision may help to reach higher performance. Nevertheless, it is challenging for most DL supervised methods to generalize well in this problem, especially when the training data are in paucity. For instance, the current state-of-the-art SSL method achieves the reported performance using the full training set. According to their weakly supervision analysis [15], SSL achieves comparable performance with CBM when trained with roughly 50% of the data.

Table 2. Comparative results of different methods using the AJI on Test-2 set (6 histology images from bladder, colon, stomach) and the testing data (14 images) from the MoNuSeg Challenge, where the best performance is shown in boldface.

Method	Test-2	Challenge Data
<i>Unsupervised</i>		
Cell Profiler [18]	0.0809	0.1232
Fiji [19]	0.3030	0.2733
Self-Supervised [14]	-	0.5354
CBM (Ours)	0.5808	0.6142
<i>Supervised</i>		
CNN2 [9]	-	0.3482
CNN3 [9]	0.4989	0.5083
DCAN [10]	0.5449	-
PA-Net [11]	0.5608	-
BES-Net [20]	0.5823	-
CIA-Net [8]	0.6306	0.6907
SSL [15]	-	0.7063

Table 3. AJI performance comparison between P and L channels.

Colorspace	Test-2	Challenge Data
L	0.5414	0.5856
P	0.5808	0.6142

To illustrate the energy compaction capability of the PQR channel decomposition, we compare the AJI performance for the P channel and the L channel (in the LAB color space) in Table 3. The advantage of using the P channel is clearly demonstrated in the table.

4. CONCLUSION AND FUTURE WORK

Nuclei segmentation in histology images is a demanding and prone to errors task for physicians, and its automation is of high importance for cancer assessment. The proposed CBM method offers a promising lightweight unsupervised direction for nuclei segmentation, requiring no labeled data and no parameter cost. It addressed the problem based on data-driven color conversion and binarization, as well as a morphological module that takes into account priors about the nuclei shape and size. In the future, we would like to boost the segmentation performance furthermore by exploring weakly or self supervision.

5. REFERENCES

- [1] S. Naik, S. Doyle, S. Agner, A. Madabhushi, M. Feldman, and J. Tomaszewski, "Automated gland and nuclei segmentation for grading of prostate and breast cancer histopathology," in *2008 5th IEEE International Symposium on Biomedical Imaging: From Nano to Macro*. IEEE, 2008, pp. 284–287.
- [2] K. Y. Win and S. Choomchuay, "Automated segmentation of cell nuclei in cytology pleural fluid images using otsu thresholding," in *2017 International Conference on Digital Arts, Media and Technology (ICDAMT)*. IEEE, 2017, pp. 14–18.
- [3] J.-P. Thiran and B. Macq, "Morphological feature extraction for the classification of digital images of cancerous tissues," *IEEE Transactions on biomedical engineering*, vol. 43, no. 10, pp. 1011–1020, 1996.
- [4] T. Mouroutis, S. J. Roberts, and A. A. Bharath, "Robust cell nuclei segmentation using statistical modelling," *Bioimaging*, vol. 6, no. 2, pp. 79–91, 1998.
- [5] N. Malpica, C. O. De Solórzano, J. J. Vaquero, A. Santos, I. Vallcorba, J. M. García-Sagredo, and F. Del Pozo, "Applying watershed algorithms to the segmentation of clustered nuclei," *Cytometry: The Journal of the International Society for Analytical Cytology*, vol. 28, no. 4, pp. 289–297, 1997.
- [6] M. Veta, A. Huisman, M. A. Viergever, P. J. van Diest, and J. P. Pluim, "Marker-controlled watershed segmentation of nuclei in h&e stained breast cancer biopsy images," in *2011 IEEE international symposium on biomedical imaging: from nano to macro*. IEEE, 2011, pp. 618–621.
- [7] S. Ali, R. Veltri, J. I. Epstein, C. Christudass, and A. Madabhushi, "Adaptive energy selective active contour with shape priors for nuclear segmentation and gleason grading of prostate cancer," in *International Conference on Medical Image Computing and Computer-Assisted Intervention*. Springer, 2011, pp. 661–669.
- [8] Y. Zhou, O. F. Onder, Q. Dou, E. Tsougenis, H. Chen, and P.-A. Heng, "Cia-net: Robust nuclei instance segmentation with contour-aware information aggregation," in *International Conference on Information Processing in Medical Imaging*. Springer, 2019, pp. 682–693.
- [9] N. Kumar, R. Verma, S. Sharma, S. Bhargava, A. Vahadane, and A. Sethi, "A dataset and a technique for generalized nuclear segmentation for computational pathology," *IEEE transactions on medical imaging*, vol. 36, no. 7, pp. 1550–1560, 2017.
- [10] H. Chen, X. Qi, L. Yu, Q. Dou, J. Qin, and P.-A. Heng, "Dcan: Deep contour-aware networks for object instance segmentation from histology images," *Medical image analysis*, vol. 36, pp. 135–146, 2017.
- [11] S. Liu, L. Qi, H. Qin, J. Shi, and J. Jia, "Path aggregation network for instance segmentation," in *Proceedings of the IEEE conference on computer vision and pattern recognition*, 2018, pp. 8759–8768.
- [12] H. Irshad, L. Montaser-Kouhsari, G. Waltz, O. Bucur, J. Nowak, F. Dong, N. W. Knoblauch, and A. H. Beck, "Crowd-sourcing image annotation for nucleus detection and segmentation in computational pathology: evaluating experts, automated methods, and the crowd," in *Pacific symposium on bio-computing Co-chairs*. World Scientific, 2014, pp. 294–305.
- [13] H. Qu, P. Wu, Q. Huang, J. Yi, Z. Yan, K. Li, G. M. Riedlinger, S. De, S. Zhang, and D. N. Metaxas, "Weakly supervised deep nuclei segmentation using partial points annotation in histopathology images," *IEEE Transactions on Medical Imaging*, vol. 39, no. 11, pp. 3655–3666, 2020.
- [14] M. Sahasrabudhe, S. Christodoulidis, R. Salgado, S. Michiels, S. Loi, F. André, N. Paragios, and M. Vakalopoulou, "Self-supervised nuclei segmentation in histopathological images using attention," in *International Conference on Medical Image Computing and Computer-Assisted Intervention*. Springer, 2020, pp. 393–402.
- [15] X. Xie, J. Chen, Y. Li, L. Shen, K. Ma, and Y. Zheng, "Instance-aware self-supervised learning for nuclei segmentation," in *International Conference on Medical Image Computing and Computer-Assisted Intervention*. Springer, 2020, pp. 341–350.
- [16] W. Yan, Y. Wang, S. Gu, L. Huang, F. Yan, L. Xia, and Q. Tao, "The domain shift problem of medical image segmentation and vendor-adaptation by unet-gan," in *International Conference on Medical Image Computing and Computer-Assisted Intervention*. Springer, 2019, pp. 623–631.
- [17] S. Lal, D. Das, K. Alabhya, A. Kanfade, A. Kumar, and J. Kini, "Nucleisegnet: Robust deep learning architecture for the nuclei segmentation of liver cancer histopathology images," *Computers in Biology and Medicine*, vol. 128, p. 104075, 2021.
- [18] A. E. Carpenter, T. R. Jones, M. R. Lamprecht, C. Clarke, I. H. Kang, O. Friman, D. A. Guertin, J. H. Chang, R. A. Lindquist, J. Moffat *et al.*, "Cellprofiler: image analysis software for identifying and quantifying cell phenotypes," *Genome biology*, vol. 7, no. 10, pp. 1–11, 2006.
- [19] J. Schindelin, I. Arganda-Carreras, E. Frise, V. Kaynig, M. Longair, T. Pietzsch, S. Preibisch, C. Rueden, S. Saalfeld, B. Schmid *et al.*, "Fiji: an open-source platform for biological-image analysis," *Nature methods*, vol. 9, no. 7, pp. 676–682, 2012.
- [20] H. Oda, H. R. Roth, K. Chiba, J. Sokolić, T. Kitasaka, M. Oda, A. Hinoki, H. Uchida, J. A. Schnabel, and K. Mori, "Besnet: boundary-enhanced segmentation of cells in histopathological images," in *International Conference on Medical Image Computing and Computer-Assisted Intervention*. Springer, 2018, pp. 228–236.